Original Article
Hemodynamic characteristics of vertebrobasilar artery fenestration combined with vertebrobasilar dolichoectasia: a study based on magnetic resonance angiography

Xiao-Qin Chen[1], Jie Jiang[2], Jian Xing[3], Zhao-Kai Ming[4], Min Zhu[3], Quan Bao[3], Ming-Cheng Hu[3]

[1]*Department of Radiology, West China Hospital, Sichuan University, Chengdu, Sichuan, China;* [2]*Department of Infectious Diseases, Mudanjiang Forestry Central Hospital, Mudanjiang, Heilongjiang, China;* [3]*Department of Magnetic Resonance Imaging, Hongqi Hospital Affiliated to Mudanjiang Medical University, Mudanjiang, Heilongjiang, China;* [4]*Department of Radiology, The First Hospital of Qiqihar, Qiqihar, Heilongjiang, China*

Abstract: Purpose: This study delves into the hemodynamic characteristics of Vertebrobasilar Artery Fenestration (VBAF) combined with Vertebrobasilar Dolichoectasia (VBD) using Magnetic Resonance Angiography (MRA). By summarizing the hemodynamic features and identifying high-risk populations, we aim to provide insights for clinical treatment. Methods: Utilizing MRA images as a foundation, arterial three-dimensional geometric models were constructed. A total of 22 cases were categorized into control, S, L, U, and Spiral groups, and numerical simulation analysis of the vessels was conducted using computational fluid dynamics methods. Results: Hemodynamic parameters of the VBAF combined with the VBD model were obtained, including blood flow velocity, oscillatory shear stress (OSI), wall shear stress (WSS), and aneurysm formation indicator (AFI). The V, OSI, and WSS indices of the L, U, and Spiral groups were significantly higher than those of the control group ($P < 0.05$). High-speed blood flow, elevated WSS, and increased OSI in these groups were concentrated at the fenestration site, with scattered distribution along the tortuous vertebral artery and basilar artery segments, accompanied by significant differences in the parameters of the bilateral vertebral arteries. Conclusion: This preliminary investigation identifies the L, U, and Spiral groups as high-risk populations. Abnormal hemodynamics may lead to a vicious cycle in vascular wall pathology, increasing the likelihood of adverse events such as cerebral infarction. Clinical attention should focus on individuals within these groups and their corresponding vascular regions.

Keywords: Vertebrobasilar artery fenestration, vertebrobasilar dolichoectasia, hemodynamics, turbulence, cerebral infarction

Introduction

Cerebral artery fenestration is a congenital vascular anomaly resulting from the failed fusion of embryonic blood vessels, characterized by arterial lumen division and reconnection distally to form a single lumen, involving local replication of endothelial cells and media splitting [1, 2]. Cerebral artery fenestration can occur in multiple vessels, with a predilection for the vertebrobasilar arteries [3]. Vertebrobasilar Artery Fenestration (VBAF) typically ranges from 1-5 mm, and due to its small diameter, it may often be an easily overlooked cerebrovascular abnormality in clinical practice. While VBAF is rare, its association with cerebral infarction (CI), aneurysms, arteriovenous malformations, and subarachnoid hemorrhage has been reported [4].

Vertebrobasilar dolichoectasia (VBD) represents an arterial pathology characterized by the vertebral or basilar arteries' elongation, dilation, or tortuosity. VBD can lead to alterations in intracranial hemodynamics, subsequently resulting in corresponding clinical symptoms closely associated with posterior circulation ischemia and, in severe cases, cerebral infarction. Studies have indicated

that hemodynamic alterations caused by morphological changes in the vertebral or basilar arteries are significant contributors to adverse events such as CI [5]. It is currently believed that the formation of VBD may result from the interaction between arterial wall pathology and vascular mechanics, with hemodynamic forces playing a pivotal role [6]. VBD formation factors include arterial wall structure, vascular wall pressure, and wall shear stress [7].

Both VBAF and VBD alter the geometric characteristics of arteries, leading to changes in internal flow dynamics such as the formation of high-viscosity blood and stasis, which affect the biological function of endothelial cells lining the arterial walls and predispose to pathological thrombotic events, culminating in adverse events like CI [8]. Therefore, analyzing relevant hemodynamic parameters of VBAF combined with VBD is imperative. This study conducts a hemodynamic analysis of VBAF combined with VBD based on MRA, extracting hemodynamic parameters of the VBAF combined with the VBD model to understand the hemodynamic changes within abnormal vessels, extract and summarize parameter characteristics, and provide relevant evidence for clinical treatment and early intervention.

Materials and methods

Data collection

This study selected 22 patients diagnosed with VBAF combined with VBD who underwent MRA scans at the Hongqi Hospital, affiliated with Mudanjiang Medical University, between October 2022 and December 2023. Head MRA was conducted using a Philips Intera 3.0 T superconducting MR scanner with an 8-channel head coil. MRA scan parameters were as follows: TR 32 ms, TE 4 ms, slice thickness 5 mm, slice gap 1 mm, matrix 256×256, FOV 240 mm×240 mm. In previous studies, the vertebral artery (VA) or basilar artery (BA) were often separately analyzed before diagnosing vertebrobasilar dolichoectasia (VBD). There is no consistent imaging standard for defining and classifying VBD, and there has been no proposed comprehensive classification system for VBD (considering VA and BA as a whole) [9]. Building upon prior research, this study categorizes VBD based on overall vascular morphology into four preliminary types (**Figure 1**): S, L, U, and spiral types. The S-type exhibits double-reversed twists in VA and/or BA, resembling the letter "S". U-type and L-type predominantly involve BA deviating from the brainstem, with one side of VA crossing to the contralateral side and joining the contralateral VA to form the BA, resembling the letters "U" and "L". The spiral type involves severe twisting and turning of VA and/or BA, resembling a spiral shape. Inclusion criteria [10]: (1) Diagnosed with VBAF (S, L, U, and Spiral groups) via head MRA; (2) Met one of the following criteria: the length of the basilar artery exceeds 29.5 mm, or the lateral deviation distance exceeds 10 mm from the perpendicular line between the origin and bifurcation of the basilar artery; the intracranial segment of the vertebral artery exceeds 23.5 mm in length, or any deviation distance of the vertebral artery exceeds 10 mm from the line between the intracranial entrance of the vertebral artery and the origin of the basilar artery; (3) High-quality MRA reconstruction models suitable for hemodynamic analysis. Exclusion criteria [11]: (1) Presence of other vascular malformations, intracranial tumors, or conditions affecting arterial blood flow; (2) Concurrent severe cardiac, pulmonary, hepatic, or renal dysfunction. Examination data were uniformly stored in the international standard DICOM format on CDs. The research protocol was approved by the Medical Ethics Committee of Mudanjiang Medical University.

Model reconstruction

MRA images were processed using the advanced visualization software MIMICS (Materialise, Belgium) to generate three-dimensional models of VBAF combined with VBD. This software utilizes DICOM (Digital Imaging and Communications in Medicine) format MRA images to create spatial reconstructions of the vascular system. The region of interest was segmented using threshold seg-

mentation, with manual delineation of certain vessels, and three-dimensional reconstructions were confirmed based on multi-planar views to ensure accurate measurements. The reconstructed model was saved in STL format and imported into 3-MATIC software (Materialise, Belgium) for model smoothing and quality diagnostics. After obtaining qualified models, they were saved in STL format. The vertebrobasilar arteries were treated as a whole [12], and the datasets were divided into five groups based on the degree of vertebral basilar artery tortuosity and vascular morphology, namely: "Control group, S group, L group, U group, and Spiral group", as shown in **Figure 1**.

Mesh generation

The model was imported into ANSYS FLUENT MESHING (ANSYS, USA) software to define a model inlet and outlet boundaries, meshing surface and volume grids, and optimize. The number of grids for all models ranged from 329,465 to 664,605, with model properties set to fluid for subsequent computational analysis. To ensure the accuracy of the results, the model underwent six-layer boundary layer refinement.

Boundary conditions and computational settings

The numerical simulation assumed that the vertebrobasilar artery wall was rigid, and blood was modeled as laminar flow with Newtonian fluid properties [13]. The boundary condition at the vertebrobasilar artery wall inlet was set as velocity inlet. The study employed blood density $\rho=1060$ kg/m³ and blood viscosity of 0.0035 Pa·s, and computational simulations were performed using Fluent software (ANSYS, USA) [14].

Statistical analysis

The final data of the last cardiac cycle obtained from the above calculations were imported into ENSIGHT (CEI, USA), with random sampling (20 sampling points) in the fenestration area. Four hemodynamic parameters, namely Velocity (V), Aneurysm formation indicator (AFI), Oscillatory shear index (OSI), and Wall shear stress (WSS) were selected for comparison analysis among the five groups. Statistical analysis was performed using SPSS 26.0 software, including tests for normality and homogeneity of variance. Normally distributed and homogenous quantitative data were expressed as mean ± standard deviation, while non-normally distributed or heterogeneous quantitative data were expressed as median (quartile). Group comparisons of quantitative data were conducted using analysis of variance for normally distributed data and the Kruskal-Wallis rank-sum test for non-normally distributed data. Count data were analyzed using Fisher's exact probability method. A significance level of $P < 0.05$ was considered statistically significant.
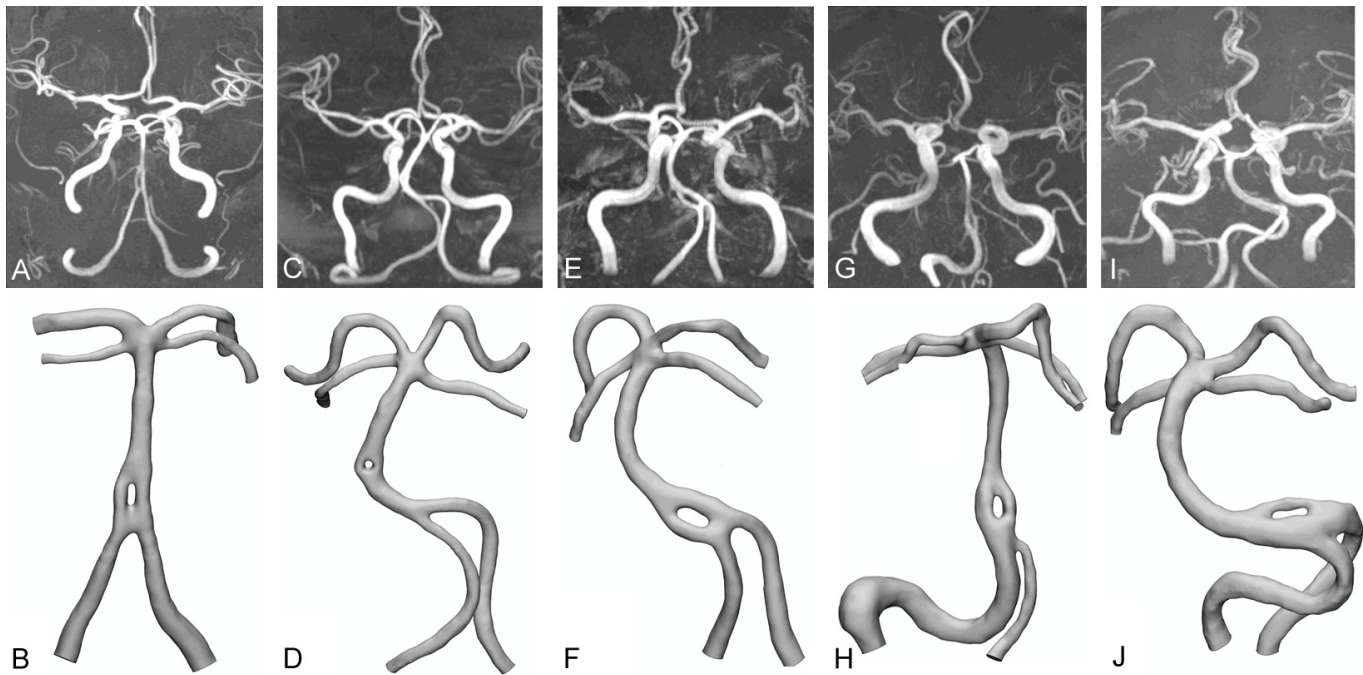
Figure 1. Displaying different groups. The top row shows maximum intensity projection images, while the bottom row displays the three-dimensional reconstructed models. A, B. Control Group; C, D. S Group; E, F. L Group; G, H. U Group; I, J. Spiral Group.

Table 1. Comparison of baseline characteristics among groups

Variables	Control Group (n=6)	S Group (n=3)	L Group (n=5)	L Group (n=5)	Spiral Group (n=3)	Statistical analysis	P
Age (years)	61.83 ± 10.68	71.00 ± 3.61	69.20 ± 6.61	70.40 ± 4.04	67.00 ± 1.00	1.45	0.26
Male	1 (17%)	2 (67%)	1 (20%)	3 (60%)	2 (67%)	4.64	0.37
Hyperlipidemia	3 (50%)	1 (33%)	2 (40%)	1 (20%)	1 (33%)	1.53	0.96
Smoking history	2 (33%)	2 (67%)	4 (80%)	3 (60%)	2 (67%)	2.81	0.75
Hypertension history	4 (66%)	2 (67%)	2 (40%)	3 (60%)	1 (33%)	1.85	0.89
Diabetes history	5 (84%)	1 (33%)	4 (80%)	2 (40%)	2 (67%)	3.94	0.46
Alcohol consumption history	3 (50%)	1 (33%)	4 (80%)	1 (20%)	1 (33%)	4.05	0.47

Results

General characteristics

The general characteristics, including clinical age, gender, history of hyperlipidemia, smoking, hypertension, diabetes, and alcohol consumption among the five groups, were compared using analysis of variance or Fisher's exact test (**Table 1**). No statistically significant differences were observed ($P > 0.05$).

Comparison of blood flow velocity among groups

As depicted in **Figure 2**, the hemodynamic parameter V in the L, U, and Spiral groups surpasses that of the control group, with statistical significance ($P < 0.05$). **Figure 3** illustrates the variation in hemodynamic parameters across different groupings. The control and S groups exhibit relatively lower and stable blood flow velocities without apparent turbulence or disturbed flow (0.10 ±

0.04 m/s, 0.18 ± 0.06 m/s). Conversely, the velocities in the U, L, and Spiral groups progressively accelerate (0.30 ± 0.05 m/s, 0.30 ± 0.07 m/s, 0.32 ± 0.01 m/s), indicating heightened complexity in blood flow patterns. In the L group, high-velocity blood flow is observed from the fenestration site to the basilar artery, albeit without evident turbulence. The U group manifests high-velocity blood flow areas in the vertebral arteries, fenestration site, and basilar artery segment, accompanied by minor turbulence and substantial disparity in blood flow velocities between bilateral vertebral arteries. Notably, the Spiral group exhibits high-velocity blood flow and turbulence in the basilar artery segment, extending across a broader range than preceding groups, with the fenestration site being the focal point.

Comparison of OSI among groups

As depicted in **Figure 2**, OSI parameters of the L, U, and Spiral groups were significantly higher than those of the
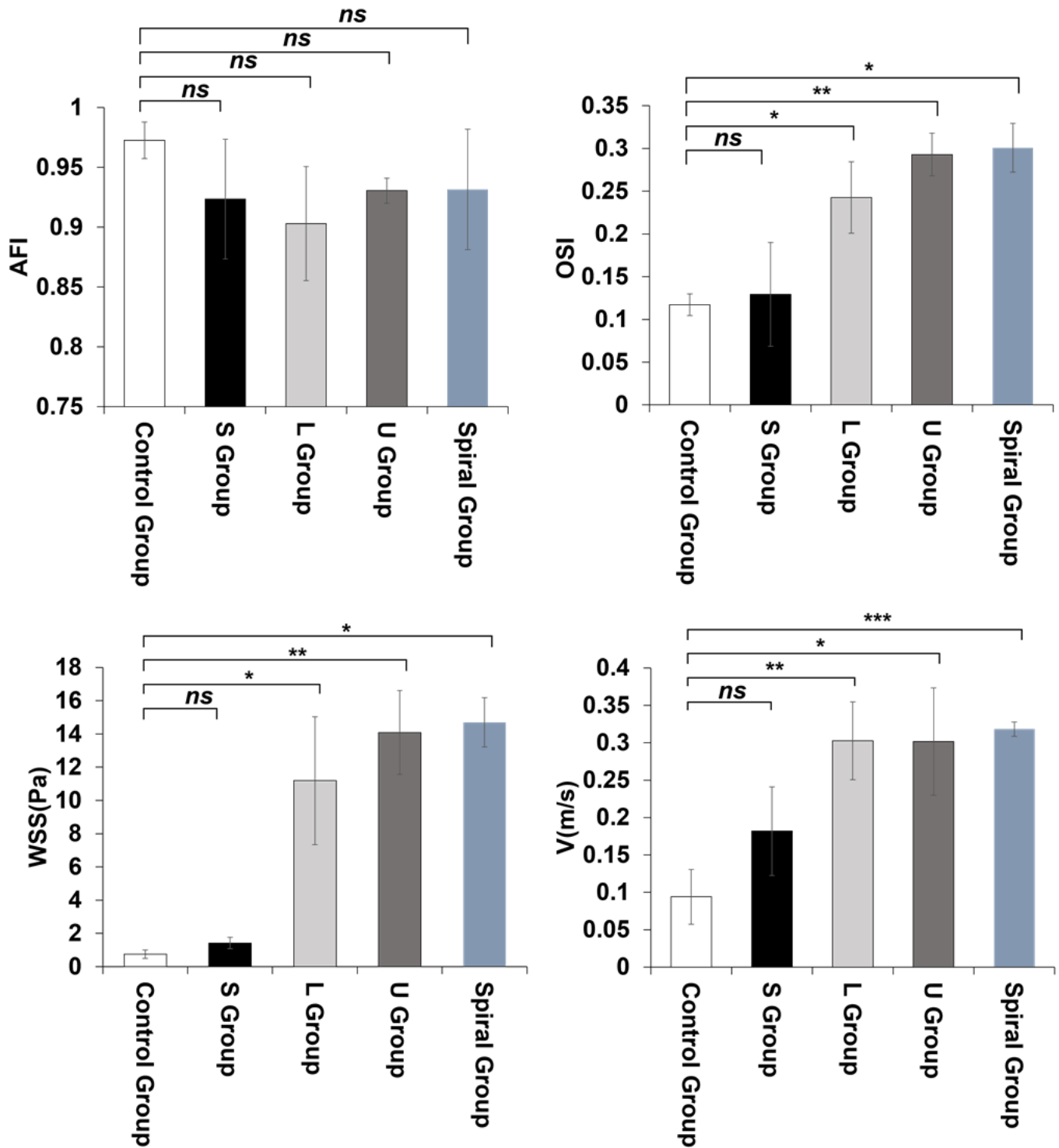
Figure 2. Bar chart illustrating hemodynamic parameters across groups. The hemodynamic parameters V, OSI, and WSS in the L, U, and Spiral groups are higher than those in the control group, with statistical significance (P < 0.05). However, the AFI parameter does not show statistical significance between groups (P > 0.05). *ns, not significant, P ≥ 0.05; *, P < 0.05; **, P < 0.01; ***, P < 0.001.*

Control group, with statistical significance (*P* < 0.05). **Figure 3** reveals that OSI variations in each group were concentrated at the fenestration and the terminal bifurcation area of the basilar artery, with minimal changes observed in other vessels. The Control and S groups exhibited lower overall OSI values, showing no significant abnormal fluctuations (0.12 ± 0.01, 0.13 ± 0.06). In the L

group, high OSI values were observed at the fenestration origin, confluence, and the terminal segment of the basilar artery (0.24 ± 0.04), with no other noticeable anomalies. The U group showed high OSI values at the commencement of the vertebral artery, fenestration, and mid-segment of the basilar artery (0.29 ± 0.03), accompanied by significant differences in WSS between
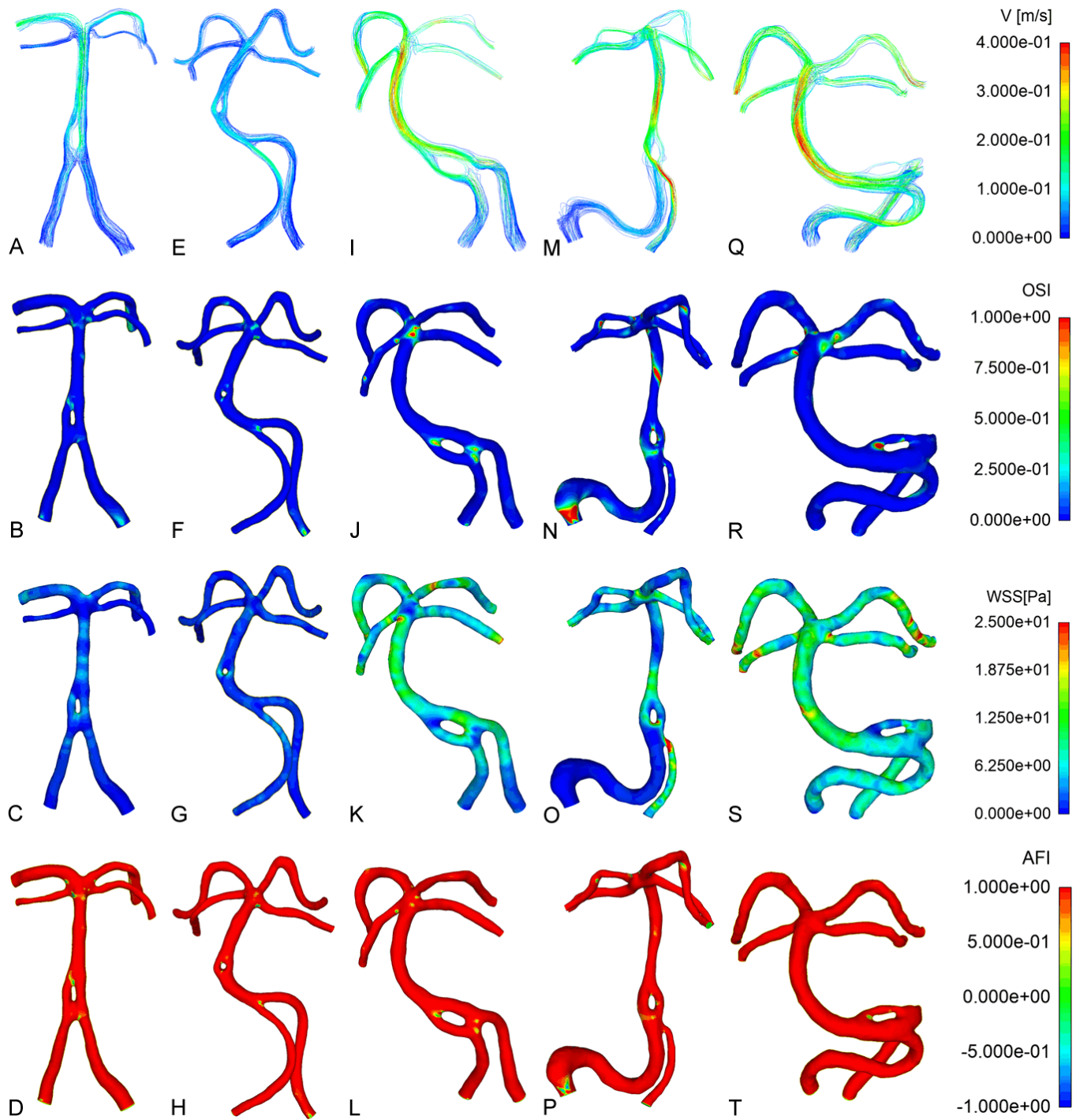
Figure 3. Model graphs of hemodynamic parameters for each group. The first row displays images of V, the second row shows OSI, the third row illustrates WSS, and the fourth row presents AFI. A-D. Control Group; E-H. S Group; I-L. L Group; M-P. U Group; Q-T. Spiral Group. The Control Group and S Group show similar parameter values. For V, the L, U, and Spiral groups exhibit higher values in both VA and BA compared to the Control Group. In terms of OSI, high OSI values in the L, U, and Spiral groups are primarily concentrated at the fenestration and the distal segments of the BA. For WSS, elevated WSS is observed in specific segments of VA and BA in the L, U, and Spiral groups. The AFI values are similar across all groups. Detailed statistical differences can be found in **Figure 2**. Note: VA, Vertebral Artery; BA, Basilar Artery.

the bilateral vertebral arteries. In the Spiral group, elevated OSI was concentrated at the fenestration and the commencement of the posterior cerebral artery, with relatively higher numerical values (0.30 ± 0.03).

Comparison of WSS across groups

Figure 2 illustrates that the hemodynamic WSS parameters in the U, L, and Spiral groups are all higher than those

in the Control group, with statistically significant differences ($P < 0.05$). As depicted in **Figure 3**, the elevated WSS in the L, U, and Spiral groups mainly concentrates on the fenestration and bifurcation of the basilar artery. The Control and S groups exhibit low WSS values, with no significant elevation observed (0.75 ± 0.25 Pa, 1.42 ± 0.34 Pa). The WSS values and range gradually increase in the U, L, and Spiral groups (11.19 ± 3.84 Pa, 14.08 ± 2.52 Pa, 14.70 ± 1.48 Pa). The overall vascular performance in the L group manifests as high WSS, whereas, in the U group, high WSS is concentrated on one side of the vertebral artery and at the fenestration, accompanied by significant differences in WSS between the bilateral vertebral arteries. Moreover, the Spiral group exhibits higher overall WSS values, with significant fluctuations in WSS at the fenestration.

Comparison of AFI across groups

The differences in AFI values among the groups were not statistically significant ($P < 0.05$), as illustrated in **Figure 2**. However, **Figure 3** reveals that variations in AFI within different groups are primarily concentrated at the fenestration and vessel bifurcation sites. All groups exhibit elevated AFI values, with no significant instances of low AFI values observed. Specifically, the control group recorded a mean AFI of 0.97 ± 0.01, the S group had a mean AFI of 0.92 ± 0.05, the L group exhibited a mean AFI of 0.90 ± 0.05, the U group showed a mean AFI of 0.93 ± 0.01, and the Spiral group displayed a mean AFI of 0.93 ± 0.05.

Discussion

VBAF and VBD are both rare vascular anomalies closely associated with pathological events such as cerebral infarction and aneurysm, yet their mechanisms remain elusive [15]. It is speculated that they are largely linked to atherosclerotic changes in arterial walls induced by hemodynamic abnormalities. However, scant research exists on the hemodynamic correlation between these two conditions. The coexistence of VBAF and VBD can lead to hemodynamic alterations in intracranial blood flow, subsequently resulting in corresponding clinical symptoms and complications such as subarachnoid hemorrhage. Given the acute onset and short window for effective intervention, these conditions negatively impact patients, severely compromising their quality of life [16]. Hence, understanding the risk mechanisms of VBAF combined with VBD and being able to predict, diagnose early, and intervene promptly hold significant clinical implications. In this study, utilizing MRA imaging data and mechanical modeling software, we conducted three-dimensional post-processing of VBAF combined with VBD image data of various morphologies, analyzing the hemodynamic aberrations associated with these conditions.

Computer simulation analysis is an effective method for evaluating hemodynamics in the human vasculature. It provides hemodynamic parameters that are difficult to obtain in animal and basic experiments and visually displays them to analyze early hemodynamic changes in VBAF combined with VBD. Therefore, based on real patient image data in this study, we established three-dimensional vascular models and divided them into different groups to discuss hemodynamic parameters, identifying differences among groups and identifying high-risk populations for VBAF combined with VBD, thus providing guidance for early treatment.

Regarding the V aspect, high-speed blood flow in Groups L, U, and Spiral is distributed in the tortuous vertebral arteries, fenestrations, and the basilar artery, with turbulent flow observed at the fenestrations. Structural anomalies in this study's fenestrations and vertebral basilar arteries increase the complexity of hemodynamics compared to normal vessels. Normal blood flow within vessels exhibits laminar flow, with slightly higher velocity flow in the center and lower velocity flow in the periphery [17]. This pattern facilitates the effective transport of substances within the blood, reduces friction with the vessel wall, and prevents the deposition of atherosclerotic substances on the vessel wall [18, 19]. It has been found that turbulent flow and plaque formation are more likely to occur at arterial branches, bifurcations, and curvatures. In Groups L, U, and Spiral, turbulent flow is observed in the tortuous vertebral arteries, fenestrations, and the basilar artery, disrupting normal blood flow patterns, facilitating the transport of atherosclerotic factors to the vessel wall, and increasing the probability and severity of inflammatory reactions. The study by Mei et al [20] also suggests that a significant increase in arterial velocity promotes the formation of atherosclerosis and simultaneously affects the healing process after treatment, further corroborating the findings of this study.

Regarding OSI, with values ranging from 0 to 1, it is a dimensionless parameter indicating the degree of change in blood flow direction. Higher OSI values indicate greater changes in blood flow direction, even retrograde flow, whereas lower values signify stable blood flow, indicating normal flow conditions with stable flow intensity and direction [21]. Higher OSI values imply greater changes in wall shear stress direction, which are more related to disturbances in the flow field within the vessel [22]. In our experiment, high OSI values in Groups L, U, and Spiral are predominantly located at the fenestrations, with scattered high OSI values in the vertebral and basilar arteries. High OSI reduces effective blood flow within the vessel lumen, increases kinetic energy loss, shortens the proliferation and apoptosis cycle of endothelial cells, and increases endothelial cell lipid uptake, disrupting normal endothelial cell physiological processes, disturbing the balance between active protective factors and vascular injury factors, and leading to vascular wall degeneration, thereby increasing the probability and severity of inflammatory reactions [23]. Tong et al [24] built hypothetical fenestration models based on normal basilar artery models of different sizes and positions. They found that an

increase in OSI values at the fenestration site correlates with a higher risk of adverse events such as stroke formation.

Regarding WSS, high WSS in Groups L, U, and Spiral is observed at the fenestrations and the basilar artery segment, partially overlapping with high-speed blood flow areas, with significant differences in WSS in some vessels. During blood flow, the energy carried by the blood gradually converts into force acting on the vessel wall, with WSS being the primary force proportional to blood flow velocity. It is currently believed that high WSS increases the risk of events such as cerebral infarction [25]. As blood flow velocity increases, WSS significantly rises, exceeding a certain threshold, leading to vascular wall damage, recruitment of numerous inflammatory cells to the damaged vessel wall, and a series of inflammatory reactions. This continuous cycle of disruption destabilizes the vessel wall, making it unable to maintain its basic form and function, thereby increasing the risk of wall rupture and other events [26]. Endothelial cell damage, disruption of the internal elastic lamina, recruitment of numerous inflammatory cells to the weakened part of the vessel wall, hypoxia in the medial layer of the arterial wall, vascular necrosis, endothelial cell damage, driving inflammatory cascade reactions, further aggravate vessel wall damage. Consistent with previous studies, Xu et al [27] also found that arterial velocity and WSS significantly increase the risk of unstable arterial wall rupture and affect the post-treatment healing condition of the vessels. The study by Lescher et al [28] showed that high WSS may increase the risk of vascular wall rupture, further supporting the findings of this study.

Regarding AFI, the vascular changes in each group are concentrated at the fenestrations and vessel bifurcations, with all groups exhibiting high AFI, and no significant low AFI values observed. AFI refers to the specific value measured by the angle between the instantaneous WSS and the mean vector direction at any given moment [29]. A smaller AFI value indicates that the WSS vector direction is closer to 90°, indicating significant abnormal blood flow changes at this location, increased wall stress variation, and worsened hemodynamics.

This study utilized post-processing software to simulate local blood vessels in the human body. Although real patient imaging data was collected, the study's retrospective nature precluded the specific collection of boundary conditions for each patient, potentially overlooking the influence of individual differences on blood flow. In this study, blood flow was assumed to be a Newtonian fluid. However, blood flow properties within arteries approximate Newtonian fluids. Human blood flow is actually a non-Newtonian fluid, which will be gradually improved in future research [30].

Conclusion

This preliminary investigation identifies the L, U, and Spiral groups as high-risk populations. Abnormal hemo-

dynamics may lead to a vicious cycle in vascular wall pathology, increasing the likelihood of adverse events such as cerebral infarction. Clinical attention should focus on individuals within these groups and their corresponding vascular regions.

Disclosure of conflict of interest

None.

Address correspondence to: Ming-Cheng Hu, Department of Magnetic Resonance Imaging, Hongqi Hospital Affiliated to Mudanjiang Medical University, No. 3 Tongxiang Street, Aimin District, Mudanjiang, Heilongjiang, China. Tel: +86-182-49357899; E-mail: 511582710@qq.com

References

[1] Gailloud P, Albayram S, Fasel JH, Beauchamp NJ and Murphy KJ. Angiographic and embryologic considerations in five cases of middle cerebral artery fenestration. AJNR Am J Neuroradiol 2002; 23: 585-587.

[2] Kathuria S, Gregg L, Chen J and Gandhi D. Normal cerebral arterial development and variations. Semin Ultrasound CT MR 2011; 32: 242-51.

[3] Kloska SP, Schlegel PM, Sträter R and Niederstadt TU. Causality of pediatric brainstem infarction and basilar artery fenestration? Pediatr Neurol 2006; 35: 436-438.

[4] Palazzo P, Ruff M, Lyerly MJ and Alexandrov AV. Basilar artery thrombus vs. fenestration: a differential diagnostic challenge in acute ischemic stroke. J Neuroimaging 2014; 24: 607-609.

[5] Chen W, Yi T, Chen Y, Zhang M, Wu Z, Wu Y, Chen B, Guo T, Wu C, Yang M, Chen X and Shi Y. Assessment of bilateral cerebral peduncular infarction: magnetic resonance imaging, clinical features, and prognosis. J Neurol Sci 2015; 357: 131-5.

[6] Miyamoto N, Ueno Y, Hira K, Kijima C, Nakajima S, Yamashiro K and Hattori N. Characteristics of clinical symptoms, cerebral images and stroke etiology in vertebro-basilar artery fenestration-related infarction. Brain Sci 2020; 10: 243.

[7] Scherer A, Siebler M and Aulich A. Virtual arterial endoscopy as a diagnostic aid in a patient with basilar artery fenestration and thromboembolic pontine infarct. AJNR Am J Neuroradiol 2002; 23: 1237-9.

[8] Ma W, Cheng Z, Chen X, Huang C, Yu G and Chen G. Multiphase flow hemodynamic evaluation of vertebral artery stenosis lesions and plaque stability. Biomed Mater Eng 2023; 34: 247-260.

[9] Wang Y and Yu J. Prospects and dilemmas of endovascular treatment for vertebrobasilar dolichoectasia. Front Neurol 2022; 13: 895527.

[10] Yu J, Li ML, Xu YY, Wu SW, Lou M, Mu XT, Feng F, Gao S and Xu WH. Plaque distribution of low-grade basilar artery atherosclerosis and its clinical relevance. BMC Neurol 2017; 17: 8.

[11] Chueh JY, Vedantham S, Wakhloo AK, Carniato SL, Puri AS, Bzura C, Coffin S, Bogdanov AA Jr and Gounis MJ. Aneurysm permeability following coil embolization: packing density and coil distribution. J Neurointerv Surg 2015; 7: 676-81.

[12] Jing F, Huang H, Li Y and Zang P. Vertebrobasilar dolichoectasia to trigeminal neuralgia: case report. J Surg Case Rep 2024; 2024: rjad737.

[13] Matsuura K, Jin WW, Liu H and Matsumiya G. Computational fluid dynamic study of different incision length of coronary artery bypass grafting in a native coronary stenosis model. J Thorac Dis 2019; 11: 393-399.

[14] Matsumura Y, Yamanaka T, Murai T, Fujita N and Kitahara T. Orthostatic hemodynamics in the vertebral artery and blood pressure in patients with orthostatic dizziness/vertigo. Auris Nasus Larynx 2022; 49: 593-598.

[15] Hirai S, Tanaka Y, Sato H, Kato K, Kim Y, Yamamura T, Sumita K and Arai T. Quantitative collateral assessment evaluated by cerebral blood volume measured by CT perfusion in patients with acute ischemic stroke. J Stroke Cerebrovasc Dis 2021; 30: 105797.

[16] Zhang DP, Peng YF, Zhang HL, Ma JG, Zhao M, Yin S and Wei TT. Basilar artery tortuosity is associated with white matter hyperintensities by TIMP-1. Front Neurosci 2019; 13: 836.

[17] Alexander MD, Yuan C, Rutman A, Tirschwell DL, Palagallo G, Gandhi D, Sekhar LN and Mossa-Basha M. High-resolution intracranial vessel wall imaging: imaging beyond the lumen. J Neurol Neurosurg Psychiatry 2016; 87: 589-97.

[18] Huang R, Zhang X, Chen W, Lin J, Chai Z and Yi X. Stroke subtypes and topographic locations associated with neurological deterioration in acute isolated pontine infarction. J Stroke Cerebrovasc Dis 2016; 25: 206-213.

[19] Lauric A, Hippelheuser J, Safain MG and Malek AM. Curvature effect on hemodynamic conditions at the inner bend of the carotid siphon and its relation to aneurysm formation. J Biomech 2014; 47: 3018-27.

[20] Mei Y, Guan D, Tong X, Liu Q, Hu M, Chen G and Li C. Association of cerebral infarction with vertebral arterial fenestration using non-Newtonian hemodynamic evaluation. Math Biosci Eng 2022; 19: 7076-7090.

[21] Cebral J, Ollikainen E, Chung BJ, Mut F, Sippola V, Jahromi BR, Tulamo R, Hernesniemi J, Niemelä M, Robertson A and Frösen J. Flow conditions in the intracranial aneurysm lumen are associated with inflammation and degenerative changes of the aneurysm wall. AJNR Am J Neuroradiol 2017; 38: 119-126.

[22] Riccardello GJ Jr, Changa AR, Al-Mufti F, Singh IP, Gandhi C, Roman M and Prestigiacomo CJ. Hemodynamic impingement and the initiation of intracranial side-wall aneurysms. Interv Neuroradiol 2018; 24: 288-296.

[23] Wang Y, Feng Y, Wang T, Ma Y, Gao P, Chen J, Chen Y, Yang B and Jiao L. Drug-coated balloon for vertebral artery origin stenosis: a pilot study. J Neurointerv Surg 2021; 13: 827-830.

[24] Tong X, Dong J, Zhou G, Zhang X, Wang A, Ji Z, Jiao L, Mei Y and Chen D. Hemodynamic effects of size and location of basilar artery fenestrations associated to pathological implications. Int J Numer Method Biomed Eng 2021; 37: e3507.

[25] Wang F, Xu B, Sun Z, Wu C and Zhang X. Wall shear stress in intracranial aneurysms and adjacent arteries. Neural Regen Res 2013; 8: 1007-15.

[26] Meng H, Tutino VM, Xiang J and Siddiqui A. High WSS or low WSS? Complex interactions of hemodynamics with intracranial aneurysm initiation, growth, and rupture: toward a unifying hypothesis. AJNR Am J Neuroradiol 2014; 35: 1254-1262.

[27] Xu J, Yu Y, Wu X, Wu Y, Jiang C, Wang S, Huang Q and Liu J. Morphological and hemodynamic analysis of mirror posterior communicating artery aneurysms. PLoS One 2013; 8: e55413.

[28] Lescher S, Zimmermann M, Konczalla J, Deller T, Porto L, Seifert V and Berkefeld J. Evaluation of the perforators of the anterior communicating artery (AComA) using routine cerebral 3D rotational angiography. J Neurointerv Surg 2016; 8: 1061-1066.

[29] Liu Q, Zhang Y, Yang J, Yang Y, Li M, Chen S, Jiang P, Wang N, Zhang Y, Liu J, Wu J and Wang S. The relationship of morphological-hemodynamic characteristics, inflammation, and remodeling of aneurysm wall in unruptured intracranial aneurysms. Transl Stroke Res 2022; 13: 88-99.

[30] Can A and Du R. Association of hemodynamic factors with intracranial aneurysm formation and rupture: systematic review and meta-analysis. Neurosurgery 2016; 78: 510-20.